JOURNAL OF THE ROYAL SOCIETY Interface

CrossMark click for updates

J. R. Soc. Interface (2012) **9**, 3268–3278
doi:10.1098/rsif.2012.0448
Published online 25 July 2012

Collective cell migration: leadership, invasion and segregation

Alexandre J. Kabla*

Department of Engineering, University of Cambridge, Cambridge CB2 1PZ, UK

A number of biological processes, such as embryo development, cancer metastasis or wound healing, rely on cells moving in concert. The mechanisms leading to the emergence of coordinated motion remain however largely unexplored. Although biomolecular signalling is known to be involved in most occurrences of collective migration, the role of physical and mechanical interactions has only been recently investigated. In this study, a versatile framework for cell motility is implemented *in silico* in order to study the minimal requirements for the coordination of a group of epithelial cells. We find that cell motility and cell–cell mechanical interactions are sufficient to generate a broad array of behaviours commonly observed *in vitro* and *in vivo*. Cell streaming, sheet migration and susceptibility to leader cells are examples of behaviours spontaneously emerging from these simple assumptions, which might explain why collective effects are so ubiquitous in nature. The size of the population and its confinement appear, in particular, to play an important role in the coordination process. In all cases, the complex response of the population can be predicted from the knowledge of the correlation length of the velocity field measured in the bulk of the epithelial layer. This analysis provides also new insights into cancer metastasis and cell sorting, suggesting, in particular, that collective invasion might result from an emerging coordination in a system where single cells are mechanically unable to invade.

Keywords: collective migration; epithelium; wound healing; cell invasion; active matter

1. INTRODUCTION

Many biological processes involve concerted cell displacements across large length scales and time scales. These include the most fundamental transformations taking place during embryogenesis, such as gastrulation, neurulation or vasculogenesis. Common forms of concerted motions are: (i) cell intercalation, through which the tissue undergoes a significant change of shape by cells exchanging neighbours (fly germ band extension [1], vertebrate gastrulation and neurulation [2,3]) and (ii) collective migration, during which groups of cells coordinate their direction of motion with respect to surrounding tissues, travelling reliably large distances in the embryo (neural crest cells [4], fish lateral line [5]). Collective migration also occurs in adult life, often in association with regenerative processes, such as wound healing, or pathologies, such as cancer metastasis, which often takes the form of groups of cells collectively invading other tissues [6]. Unravelling the physical and biological principles driving collective cell migration is key to understanding these critical aspects of developments, as well as to trigger new therapeutic treatments for cancer. The large variability in the systems exhibiting patterns of collective migration suggests that generic principles are controlling these behaviours [7,8], and calls for an analogy with a larger class of systems [9].

More generally, collective behaviours in groups of motile individuals have been widely studied over the past 20 years, both from a theoretical and an experimental point of view. Systems considered include animal and human populations [10] as well as bacteria [11] or active biopolymers [12]. Flock models have shown that simple interactions between individuals are sufficient for coordinating their direction of motion, without a need for a directional cue [13,14]. One fundamental assumption in such models is the existence of a local spatial coupling that tends to align the direction of motion of neighbour individuals. In the context of cell populations, flock models have already demonstrated that a local mechanical coupling is enough to generate streaming patterns [15,16] and that coordination enhances the sorting dynamics of heterogeneous populations [17]. Such emerging collective effects impose a rethink of the requirements for large-scale cell coordination and, in particular, of how complex cell interactions must be so as to ensure robust migration in complex environments. One of the limiting factors at this stage is the difficulty of experimentally dissecting the contributions of mechanical and biochemical processes.

In this study, a numerical approach is introduced to overcome such a difficulty. A range of model studies, each highlighting a different aspect of *in vitro* or

*ajk61@cam.ac.uk

Electronic supplementary material is available at http://dx.doi.org/10.1098/rsif.2012.0448 or via http://rsif.royalsocietypublishing.org.

Received 22 August 2011
Accepted 5 July 2012

in vivo collective migration, are explored. These include, in particular, the transition from cohesive epithelia to mesenchymal-like cell populations, the role of population size and confinement, the integration of directional information within the population and the conditions for collective or solitary cell invasion in a surrounding tissue. Cell interactions will be purposefully limited to a small number of fundamental processes, such as adhesion, incompressibility of the cells and a time scale for the evolution of cell polarity. This approach provides, as a result, a generic framework from which the role of biomolecular signalling can be reinterpreted.

2. RESULTS AND DISCUSSION

2.1. Dense endothelial cell monolayers

The migratory patterns of cultured endothelial cell monolayers are well documented, confirming the emergence of collective behaviours such as streaming and large-scale velocity correlations [18–23]. These experiments have shown, in particular, that cell density is one of the key parameters controlling collective behaviours. *In vivo*, cells are however usually closely packed, forming small confined groups within larger tissues [7,8]. The onset of group migration then primarily involves variations of motile behaviour, adhesive properties or environmental conditions [7], rather than of cell density. The first question addressed concerns the role of these physical and mechanical parameters in the dynamics of large and dense cell populations. The effect of the population size and its mechanical environment will be subsequently studied.

The numerical tissue is made of a two-dimensional confluent layer of cells on a substrate. Cells can adhere to each other, and the resulting cohesion of the tissue is accounted for by a membrane tension, J, which is homogeneous across the population. J controls here a number of otherwise independent properties, such as the adhesion energy, the cortical tension and the amplitudes of membrane fluctuations [24]. Moreover, all cells have the same volume and cannot overlap each other. In this first section, all cells also generate the same motile force $\boldsymbol{\mu}$ on the substrate. However, each cell has its own direction of polarization $\boldsymbol{n}_i$ along which this force is produced ($|\boldsymbol{n}_i| = 1$). The population lives on a surface with periodic boundary conditions, such that if a cell leaves on the one side, it reappears on the opposite. As a result, although the system has a finite size, it nevertheless has no boundary that could influence cell trajectories. The cellular Potts model (CPM) [25], which has already demonstrated its broad biological relevance for epithelial tissues, is used to implement these rules (see §3).

No specific molecular mechanism for inter-cellular communication is considered. Only excluded volume interactions and constraints of membrane geometry cause cells to feel each other or feel any other physical obstacle. It is however assumed that there is a feedback from earlier displacements to the polarization itself: a cell tries to move along its direction of polarization, but the polarization itself evolves towards the cell's net displacement with a response time $\boldsymbol{\tau}$ (see §3), acting as a memory (or persistence) time for the cell polarization [15,16]. These assumptions are consistent with a number of recent observations [26,27], and provide a simple way to model the interaction between a cell and its mechanical environment. Szabo *et al.* [16] have used such a model to study in more detail the dynamics of endothelial cell monolayers. They have, in particular, explored the role played by the memory time $\boldsymbol{\tau}$ in the resulting streaming behaviour and successfully replicated the experimental shape of the velocity correlations in homogeneous cell populations using realistic values of the model parameters. This demonstrates the general potential of the self-propelled cellular models for the study of collective migration patterns.

The role of the motile force $\boldsymbol{\mu}$ on the dynamics of a large cell population is first considered, with an emphasis on qualitative transitions, rather than on quantitative comparisons with experimental data. In the following, the memory time $\boldsymbol{\tau}$ and noise level are kept constant. At low motile forces, no net motion is observed (see electronic supplementary material, film S1); the population essentially behaves like a cohesive epithelium, with a strong persistence of the neighbourhood relationships. At higher motile forces, a transition occurs to a regime where cells migrate on the substrate and stream over large distances (see figure 1*a* and electronic supplementary material, film S2). The spatial correlations of the velocity field quantify the structure of the streaming patterns. Considering a cell at the origin moving towards the right, the average degree of alignment between the velocity of this cell and the velocity of the cell located at $\boldsymbol{\delta r}$ is given by the function $g(\boldsymbol{\delta r})$: $g = 1$ means full alignment; $g = -1$ corresponds to cells moving in opposite directions and $g = 0$ to a non-correlated situation (see §3). Figure 1*b* shows two-dimensional colour-coded maps of correlation functions for three different values of the motile force $\boldsymbol{\mu}$.

For intermediate values of the motile force ($\boldsymbol{\mu} \approx 0.1$), strong spatial correlations in the velocity field develop, in particular, along the direction of the cell displacement (streaming), whereas displacements tend to be anti-correlated in the normal direction (meaning that streams of opposite direction are running next to each other). Such patterns are typically observed in large cell populations [16,18,20] and *in silico* [16]. When varying (at constant density) the motile force towards smaller or larger values, spatial correlations tend however to become more localized, and could decay over a couple of cell diameters. The size of the correlated domain is quantified by $\boldsymbol{\lambda}_c = 2\boldsymbol{\sigma}$, where $\boldsymbol{\sigma}$ is the standard deviation of the correlation function along the direction of the cell displacement (see §3). Figure 1*c* shows the evolution of $\boldsymbol{\lambda}_c$ as a function of the motile force. The non-monotonic evolution of the correlation length ($\boldsymbol{\lambda}_c$) shows that the dynamics of such a dense cell population involves several competing effects that will be developed further in the following sections.

2.2. Emergence of collective motility

The transition from a non-motile to a motile population can be captured by the temporal correlations of the cell velocities, or equivalently by the mean square

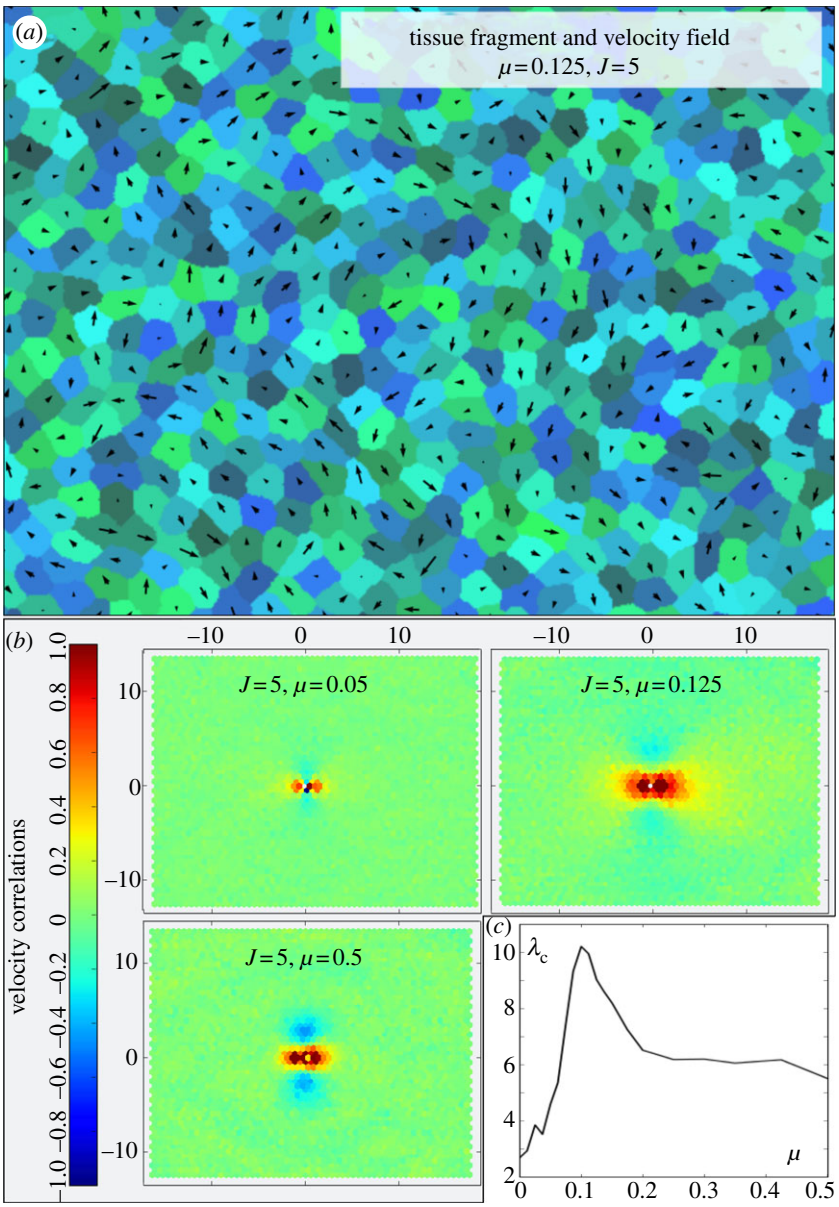

Figure 1. (*a*) An image of a motile tissue in the steady state, overlayed with the corresponding velocity field. Cell colours are arbitrary. (*b*) Maps of the velocity correlations around a cell migrating from left to right (see §3). These have been obtained for populations of 1600 cells. The unit distance is the cell diameter. (*c*) A graph of the correlation length λ_c as a function of the motile force μ, for $J = 5$.

displacement $\Delta r^2(\Delta t)$ of the cells. Figure 2 shows a selection of curves of $\Delta r^2(\Delta t)$, averaged over space and time, for a range of values of J and μ. Different classes of behaviours can be observed, depending on the value of μ/J. For low values of μ/J, while the initial behaviour is faster than diffusion (i.e. the slope in a log–log plot is larger than 1), the cell displacement strongly slows down and hardly reaches the cell size (around 20 pixels in diameter) over the time interval considered here. This corresponds to a regime where no significant relative or absolute cell displacement is observed. For larger values of μ/J, a second family of curves emerges, where the initial behaviour is now ballistic ($\Delta r^2 \propto \Delta t^2$, or equivalently $\Delta r \propto \Delta t$), and the long-term behaviour diffusive. This corresponds to a persistent random walk; the direction of migration of the cells remain essentially constant for a certain persistence time after which their trajectory becomes eventually Brownian. This corresponds to the life time of the streaming patterns discussed in §2.1. As already characterized [16], the velocity correlation time is in this regime much larger than the memory time τ of the polarization ($\tau = 10$ in these simulations).

In order to quantify the threshold between the epithelium-like and motile behaviours, the mean-square displacement curves are fitted by the function $\Delta r^2 = D\Delta t^\beta$ over the time range $10 < \Delta t < 10^4$ Monte Carlo steps (MCS; see §3). The value of β, reported in figure 2, empirically characterizes the nature of cell displacements over this particular time interval. The data confirm that β is primarily controlled by μ/J, and allows us to identify the transition point between the epithelium-like and motile regimes. For each value of J, there is a critical motile strength μ_c, scaling with J, below which transport is sub-diffusive ($\beta < 1$), i.e. where cells essentially never move more than their

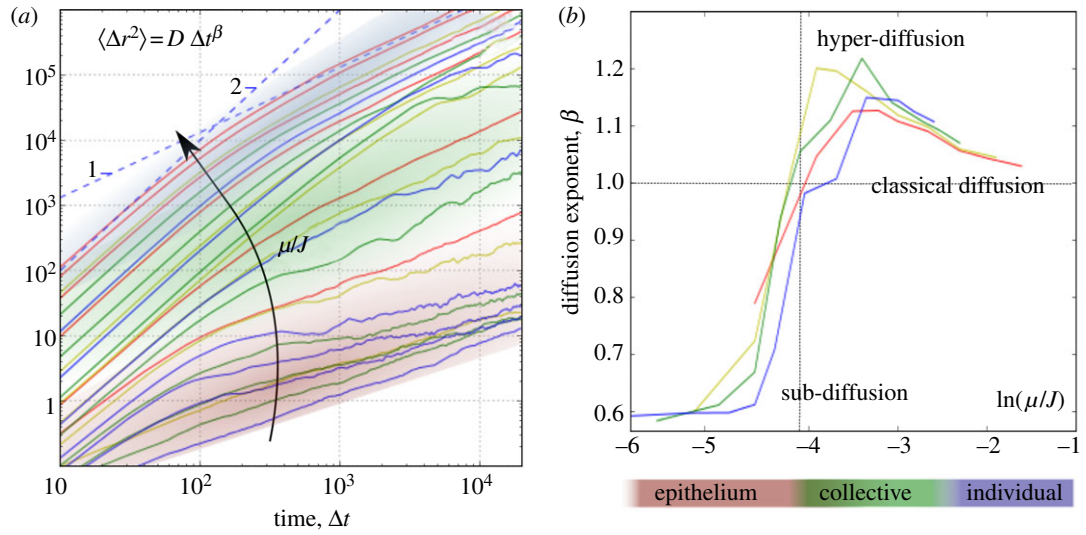

Figure 2. (*a*) Average mean-square displacement as a function of time for a range of motile force μ and adhesion J. The background colour reflects the value of μ/J, as represented on the x-axis of figure 2*b*. Distances are in pixels, and time is expressed in MCS (see §3), $\tau = 10$ MCS. The dashed lines illustrate two limit behaviours corresponding to purely diffusive ($\Delta r^2 \propto \Delta t$: slope 1) and purely ballistic ($\Delta r^2 \propto \Delta t^2$: slope 2) displacements, in order to facilitate the interpretation of the graphs. (*b*) A graph of the diffusion exponent β as a function of μ/J, for four different values of J (2.5, red; 5, yellow; 7.5, green; 10, blue). The vertical dashed line indicates the typical value of μ_c/J at which the epithelium to collective migration transition occurs.

own size. For $\mu \gtrsim \mu_c$, migration is however super-diffusive owing to the large persistence time of the cell velocity. As μ increases further, the behaviour progressively converges towards a simple diffusive behaviour, indicating that the persistence actually decreases with μ at large motile forces.

At a qualitative level, the presence of an optimum for both the spatial and temporal correlations indicates that several competing processes are taking place simultaneously. The motile force, primarily applied by a cell to the substrate, also characterizes the typical force that a cell can apply on its neighbours. Such mechanical interactions contribute to cell–cell coordination. The transition taking place when $\mu \approx \mu_c$ corresponds to the moment when large-scale coordination is achieved through this coupling. Although the motile force required for such a transition is too gentle for a cell to significantly deform its neighbours, such a process can happen as the motile force increases further, the cell becoming at some point strong enough to squeeze through them and disrupt as a result the coordination of motile groups. This partly explains why large motile forces limit the extent of collective migration. Collective migration appears therefore as an optimum where the mechanical interaction is large enough to allow a dynamical coordination of the cell polarizations, but low enough to preserve tissue integrity. The regime of high motile forces will be explored further in the context of cell invasion (§2.5).

The emergence of streaming patterns, observed in most self-propelled models, is not in itself surprising. However, interpreted within the context of a cell population, these results show (i) that local coordination can arise from purely mechanical interactions and (ii) that a number of *continuous* physical quantities, such as the motile force or the cohesion of the cellular layer, can induce abrupt transitions between *discrete* dynamical states, from a static tissue to a highly mobile population of cells, and vice versa. It appears that, even in such a simplistic model, a significant change in a tissue phenotype can originate from minute modulations of either the cells' behaviour or their environment, without a need for a cell-lineage switch or complex signalling pathways.

2.3. Emerging consensus and size effects

In vivo cases of collective migration usually involve small groups of cells with highly coordinated directions of migration, for instance, during the collective invasion of carcinoma cells, or in a number of developmental processes such a neural crest cell migration or lateral line primordium (migrating epithelium). In order to probe further the effect of the population size, systems containing 9 to 1600 cells with periodic boundary conditions have been studied. The substrate size was changed accordingly so that the cell density remained constant (see electronic supplementary material, movie S3). The degree of global coordination is quantified as the mean velocity across the whole population normalized by the mean cell speed ($\langle \boldsymbol{v} \rangle / \langle |\boldsymbol{v}| \rangle$). This corresponds to an order parameter, taking values from 0 (no order) to 1 (full coordination or sheet migration). Figure 3*a* shows how this parameter depends on the motile force, for various values of J. For each set of parameters, one can identify a typical length scale $\lambda_g(\mu, J)$ corresponding to the largest system size at which global coordination spontaneously arises. Remarkably, this length scale is similar to the λ_c measured in large cell populations (figure 1*c*). The ability to align is therefore maximum when the system is at the onset of collective

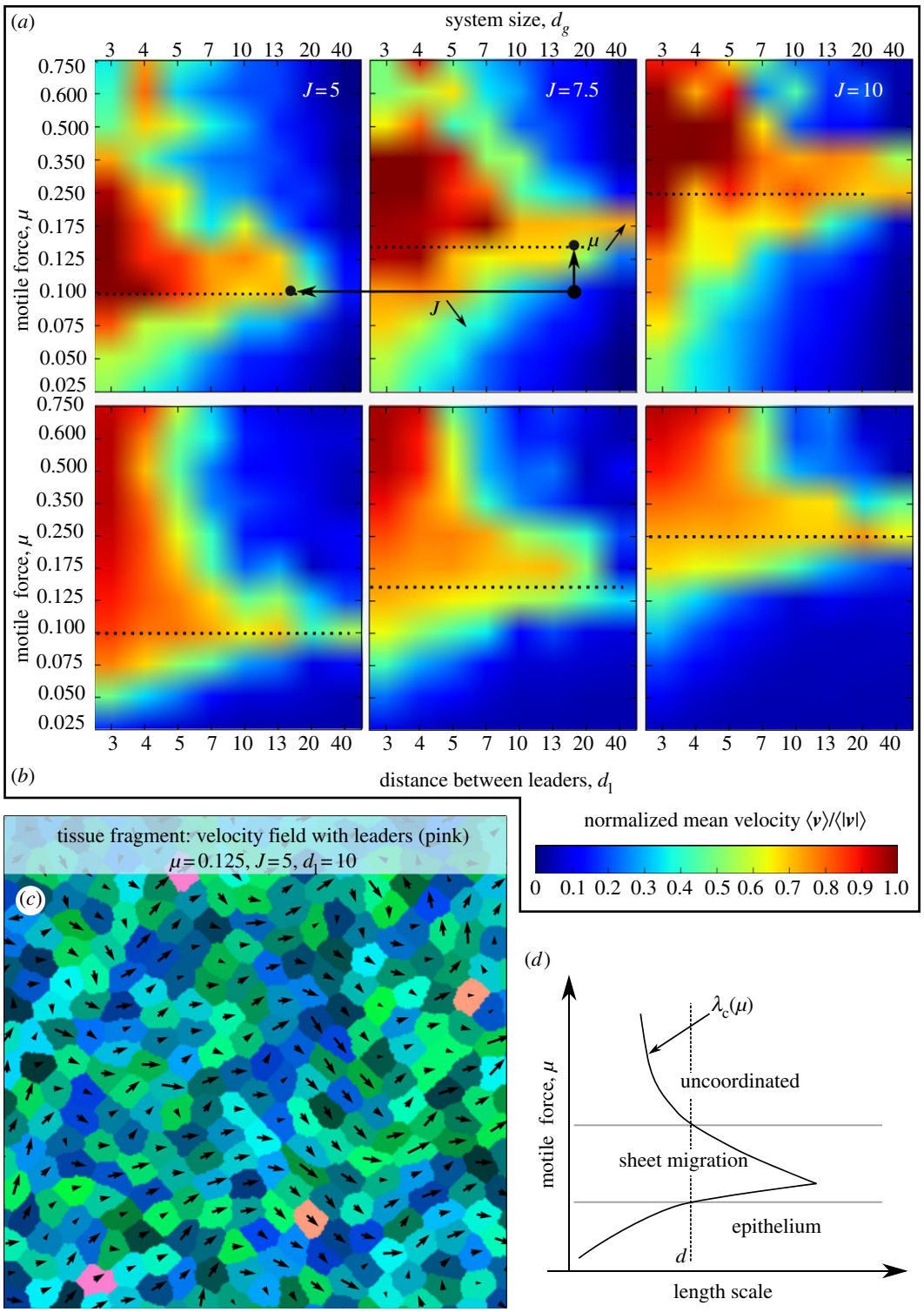

Figure 3. (a,b) Heat maps of the order parameter $\langle \boldsymbol{v}\rangle/\langle|\boldsymbol{v}|\rangle$ as a function of (a) $\boldsymbol{\mu}$ and the system size d_g (number of cells: $N \approx d_g^2$) or (b) $\boldsymbol{\mu}$ and the typical distance between leaders d_l (in cell diameters). Data for three different values of J are presented. The dashed lines indicate the value of the motile force at which the λ_c is maximal. (c) An example of a tissue with a few leader cells (with pink/orange tone) whose polarity is constant and directed towards the right. (d) A sketch of the curve $\lambda_c(\boldsymbol{\mu})$ and its qualitative relationship with the different regimes of migration. For a given length scale d associated with a constraint (distance between leaders, distance between boundaries or number N of cells in the group ($d = \sqrt{N}$)), three regimes can be defined as $\boldsymbol{\mu}$ increases: epithelium, sheet migration or uncoordinated.

migration ($\mu \gtrsim \mu_c$), i.e. when temporal and spatial correlations are at their maximum.

These size effects predict stereo-typical behaviours when biological or environmental conditions are changed. Arrows in figure 3*a* show for instance that, in a small population of 10–100 uncoordinated cells, a progressive increase of the traction force, or decrease of cohesion energy J, could trigger sheet migration without a need for specific signalling cues. This might shed light on recent observations of sheet migrations

in vivo, for instance in the fish lateral line primordium [5], where global migration is emerging without a significant loss of cell–cell junctions. *In vitro* systems offer, however, larger controls over the relevant parameters. Vedula *et al.* [28] have demonstrated that, when populations of MDCK cells are forced to migrate in 20–400 μm-wide channels, their overall migration speed and amount of coordination were strongly affected by the channel width. At a width smaller than 5–10 cell sizes, strong alignment and faster migration are observed, whereas in larger channels, cells form complex vortices and fail to align. Such a transition is consistent with figure 3*a*; for a given cell population (i.e. particular μ and J), the degree of coordination decreases with the system size, analogous here to the channel width.

2.4. Leader cells and integration of external cues

Coordination alone is, however, not enough to prescribe any particular direction of motion for the population. Setting a directional preference for a group of cells requires some level of interaction with the environment—for instance, to sense a gradient. In the context of collective migration and invasion, only a small proportion of competent (leader) cells in the population seems to be required in order to induce directed motion [19,20,29]. However, how these leaders might steer the whole population remains unclear. In the context of wound healing, such leaders are often associated with the appearance of finger instabilities [30,31]. Models have been proposed to describe the dynamics of the leading edge, based on physical, mechanical and/or biochemical interactions between cells [32–34]. However, the fact that a few leaders manage to influence the cell population over very large length scales suggests that collective effects in the bulk of the population significantly contribute to the overall dynamics. In this section, physical mechanisms by which scattered leader cells could influence large-scale migratory patterns are explored.

Within our framework, leader cells would be cells whose polarity is set by an external cue, rather than through a feedback from their previous displacement; their direction of polarity $\boldsymbol{n}$ is therefore kept constant, aligned along a fixed arbitrary direction, identical for all leader cells. These cells are otherwise indistinguishable from the other cells (including same motile force μ and tension J). In contrast to live situations where leader cells tend to be located at free boundaries, a small population of such leader cells is here scattered uniformly in the tissue (figure 3*c* and electronic supplementary material, video S4). This choice allows us to study specifically how information propagates through the population; modelling a free surface would introduce many additional parameters, which would make the process less tractable at a qualitative level.

Considering large populations (too large to spontaneously coordinate), the coordination parameter $\langle \boldsymbol{v} \rangle / \langle |\boldsymbol{v}| \rangle$ is now calculated as a function of the cell motile force μ and the distance d_l between leader cells (figure 3*b*). This distance is related to the leader density $\rho_\mathrm{l} \approx d_\mathrm{l}^{-2}$. The larger the leader density (or the smaller the distance between leaders), the stronger the resulting coordination. However, as expected from systems of self-propelled particles [35], the susceptibility of the population to leader cells strongly depends on the collective aspect of the dynamics; when $\mu \approx \mu_\mathrm{c}$, 1 per cent of leader cells are sufficient to significantly coordinate the whole cell population. As mentioned previously, one can define a length-scale for each set of parameters, $\lambda_\mathrm{l}(\mu, J)$, corresponding to the largest distance between leaders that can induce a global motion of the population. Comparing figures 1*c* and 3*b* shows that a population will follow leader cells if $d_\mathrm{l} < \lambda_\mathrm{l}(\mu, J) \approx \lambda_\mathrm{c}(\mu, J)$. The population's susceptibility to leader cells is therefore determined by the correlation length λ_c measured in the absence of leader cells. The population's response to leader cells primarily depends on its own internal dynamics, and does not require explicit communication between leaders and non-leaders. This observation can be explained by the fact that each leader cell influences the dynamics of the cells present within a domain of diameter λ_c around it. If the density of leader cells is larger than one for every λ_c^2, global coordination will be achieved. More generally, this argument can be applied to all situations where constraints are associated with a particular length scale (confinement, density of local perturbation, etc). How this length scale compares with the λ_c of the unperturbed population will control the ability of the system to coordinate over macroscopic scales (figure 3*d*).

Another implication of this model is that neither specific mechanisms of communication between leaders and normal cells, nor a long-range mechanical coupling through the substrate [21] are required for large-scale coordination; the same short-range mechanical interactions are enough to serve that purpose. The idea that simple physical–mechanical interactions could indeed play a role in the leader–follower relationship has been mentioned [5,9,19], and the results presented earlier demonstrate that such a scenario is indeed plausible. The behaviour observed is moreover in very good agreement with the *in vitro* studies of Vitorino & Meyer [20], who have shown that (i) local coordination within two-dimensional populations of endothelial cells is independent of the presence of directed migration in the population and that (ii) only a very small proportion of leader or 'pioneer' cells are required to steer the whole population of cells.

2.5. Tissue invasion

Collective forms of tissue invasion not only involve the coordination of a population of cells, but also its ability to penetrate a surrounding matrix or tissue. A number of physical and biological factors are known to influence collective invasion [6], but a general picture remains challenging to extract at this stage. For instance, both the intrinsic behaviour and the environment of cancer cells seem to determine the collective or individual nature of the invasion process. In this part, the framework introduced earlier is adapted to study cell invasion in a passive surrounding tissue. The tumour cells are essentially a population of motile cells enclosed

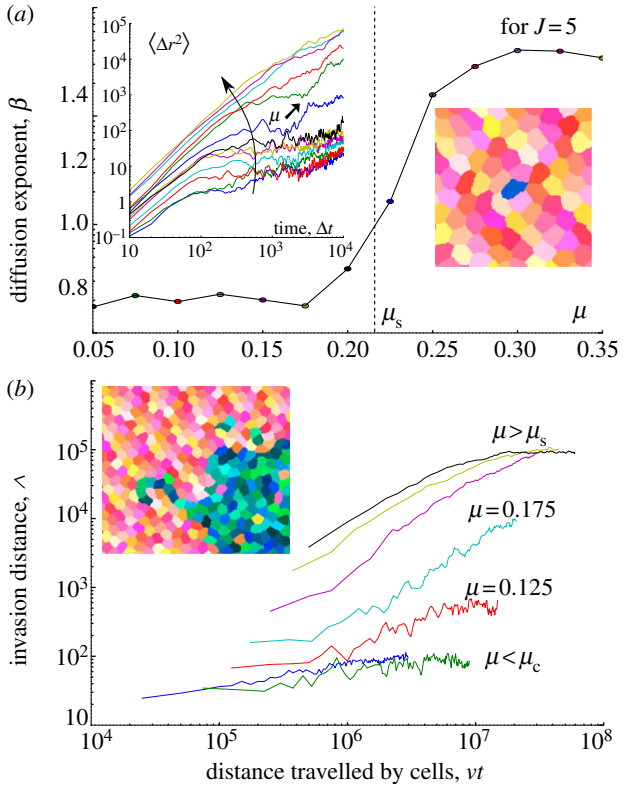

Figure 4. (*a*) Diffusion exponent β of a single motile cell in a tissue of non-motile cells. μ_s is determined by $\beta(\mu_s) = 1$. Inset: mean-square displacement of single motile cells. (*b*) A graph of the total invasion distance Λ as a function of vt, where v is the mean speed of the tumour cells; this scaling compensates for the fact that the invasion rate trivially scales with v for $\mu > \mu_s$. Data are shown for various motile forces ($J = 5$).

by a tissue. The latter is modelled for simplicity as an epithelium of non-motile cells with the same mechanical properties (encompassed by J) as the tumour cells, so that adhesion-based sorting effects will not occur [25]. J is kept constant in what follows; its role would simply be to shift the transitions as observed in figures 2 and 3. The efficiency of invasion as a function of the motile strength of the tumour cells is now characterized.

The minimal motile force μ_s required for the migration of a single cell in the passive tissue is first determined (see electronic supplementary material, movies S5–S7). Figure 4*a* shows the evolution of the mean square displacement of individual motile cells in a non-motile tissue, for a range of motile forces, and the corresponding diffusion exponent as a function of μ. $\mu_s \approx 0.22$ corresponds to the transition from a sub-diffusive behaviour (cell trapped in the tissue) to a migratory behaviour. This threshold is here larger than the motile force μ_c required for the streaming transition.

A tumour is now considered, modelled as a disc of 400 cancer cells (motile force $\mu > 0$) surrounded by thousands of non-motile tissue cells. The invasive behaviour of the tumour is quantified by a scalar quantity $\Lambda(\mu, t)$ corresponding to the sum, for all the cells which have left the tumour, of their radial distance from the initial tumour boundary, i.e. $\Lambda = \sum(r_i - R)$, where r_i is the cell distance from the tumour centre, r is the initial tumour radius and the sum is over all cells with $r_i > R$. This quantity captures both the distance travelled and the number of cells migrating away. The time evolution of this quantity for a range of motile strengths is reported in figure 4*b*. For low cancer cell motile force ($\mu < \mu_c$), cells are not migrating and no invasion occurs. For high motile force ($\mu > \mu_s$), cells are motile enough to escape individually, leading to a very efficient invasion with a linear evolution of the invasion distance Λ with time (see electronic supplementary material, movie S10). Cells eventually fully disperse in the tissue, and Λ reaches a plateau owing to the finite size of the system. Although individual cells cannot invade when $\mu < \mu_s$, a significant amount of invasion however takes place in the range $\mu_c < \mu < \mu_s$. In this regime, the invasion rate is low, but Λ increases nevertheless linearly with time. Such a discrepancy can be explained only by the emergence of a collective type of invasion. Indeed, when $\mu_c < \mu < \mu_s$, transient trains of five to 10 cells are frequently seen leaving the tumour together (see inset in figure 4*b* and electronic supplementary material, movies S8 and S9). Along these streams, cells manage to generate larger forces by pushing on each other, exceeding eventually the force required to penetrate the surrounding tissue. In this model, such an effect is made possible, thanks to emerging gradients in the cell pressure along the streams (i.e. spatial variations of the excess or lack of cell area compared with the preferred cell area). This picture is therefore analogous to the 'tug of war' process observed *in vitro* by Trepat *et al.* [36]. Collective invasion is favoured in this regime because single cell invasion is mechanically impossible, but small groups of cells can nevertheless coordinate and join forces.

Although real tumour invasions are far more complex than the processes studied here, the typical patterns of collective invasion require only straightforward conditions: (i) an ability to coordinate cell migration (through the mechanisms suggested earlier, or otherwise) and (ii) a mechanical environment (surrounding tissue, or extracellular matrix) that can resist single cell invasion but fails if the force is slightly higher. This might explain why a particular cell type could exhibit different invasion strategies depending on the properties of its direct environment (represented here by μ_s), as often observed [6]. This also suggests that having a specialized cell at the tip of the invading group [6,29] is not necessary for coordination, but might be mechanically critical. In the common case of fibroblast-led invasion, collective invasion might, for instance, proceed by (i) a track being created in the matrix/surrounding tissue by the competent fibroblast cells [29] and (ii) cancer cells streaming in the new space, strongly coordinated owing to confinement in the track.

2.6. Dynamic sorting

The populations of cells considered in this study all have the same membrane tension J, in order to avoid additional surface tension effects leading to cell sorting.

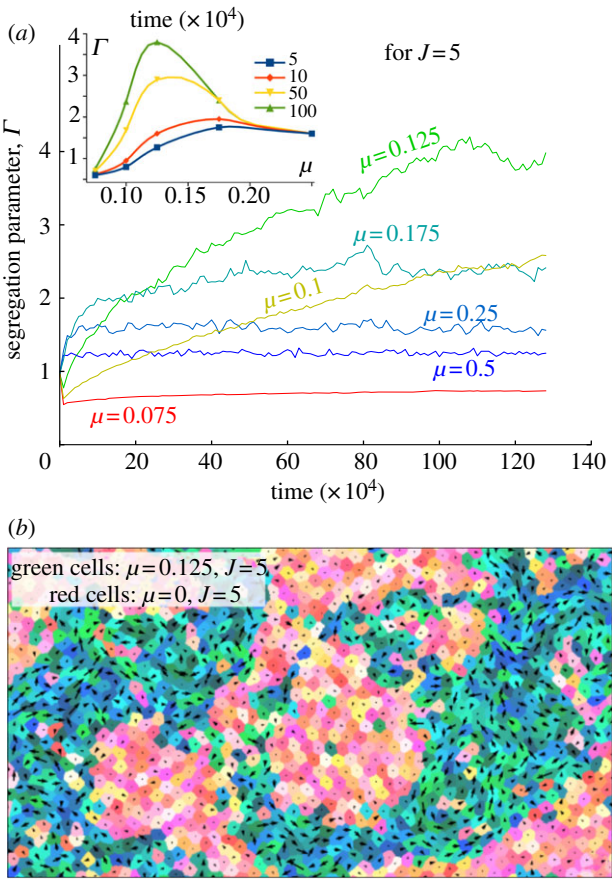

Figure 5. (*a*) Evolution of $\Gamma(t)$ (the number of contacts between two motile cells divided by the number of contacts between motile and non motile cells) for different motile forces μ ($J=5$). The data have been obtained on a system of 2048 motile cells and 2048 non-motile cells. Inset: the same data are used to plot $\Gamma(\mu)$ at different times. (*b*) A snapshot of the segregating tissue at $t=10^6$ MCS with $\mu=0.125$ and $J=5$.

Indeed, depending on the relative affinity of the different cell populations, mixing might be enhanced or prevented, interfering with the qualitative behaviour studied in this study. In fact, invasion and sorting are strongly related phenomena: a poor ability to invade is analogous to a strong tendency to segregate.

To explore this analogy further, cell sorting is now studied in a system containing an equal proportion of motile and non-motile cells, initially arranged in a chessboard pattern. Cell sorting is monitored by calculating $\Gamma(t,\mu)=n_{\mathrm{MM}}/n_{\mathrm{MN}}$, where n_{MM} is the number of contacts between motile cells, and n_{NM} is the number of contacts between motile and non-motile cells. A large value of Γ indicates a strong sorting effect, with large aggregates, whereas a random distribution would lead to $\Gamma=1$. The figure 5*a* shows the evolution of Γ as a function of time, for different values of the motile force μ. For $\mu<\mu_{\mathrm{c}}$, the whole tissue form a static epithelium and no sorting occurs. However, for motile forces in the vicinity of μ_{c}, cells progressively segregate, eventually leading to the formation of massive clusters of non-motile cells, surrounded by large streams of motile cells (see figure 5*b* and electronic supplementary material, film S11). The cluster size appears in this case to be progressively growing up to the system size, although a steady state could not be reached within the duration of the simulations. As the motile force increases further, the initial sorting rate increases, but the segregation rapidly reaches a steady regime with smaller clusters and poorer overall segregation; in this regime, motile cells are becoming invasive, which limits as a result the sorting process. The fact that the optimum segregation is reached for motile forces close to μ_{c} implies that collective effects are key in the segregation process, although no clear relationship has been identified at this stage between the λ_{c} and the cluster size and segregation dynamics.

Earlier theoretical work on cell sorting has focused on adhesion differences to explain the separation of cell populations. Although cell motile force is known to influence the dynamics of adhesion-based segregation [17], its possible role as a driving force remained unexplored. The results presented here demonstrate that differences in motility can be sufficient to drive the sorting of cell populations, even without any significant difference in adhesive properties. A distinctive signature of such a process when the two cell types are represented in similar proportions is the formation of streams of motile cells surrounding islands of non-motile groups. Some of the predictions of this model have been recently supported by *in vitro* experiments on cell co-cultures [37].

2.7. Discussion

2.7.1. A unified picture for collective migration

The practical importance of the ideas introduced here relies most of all on their ability to provide, with parsimony, a unified picture of the patterns of collective migration. This work demonstrates that a non-specific, mechanical coupling and a persistence time in the polarization direction of the cells are enough to reproduce a wide array of cellular behaviours commonly observed *in vitro* and *in vivo*. It reproduces the main features of the *in vitro* behaviour of endothelial cells away from a wound, and explains the mechanisms of large-scale coordination when a wound is present. It shows that sheet migration is a robust feature of small groups of migrating cells, and predicts that size effects and susceptibility to directional information are related to the collective dynamics of the population in an unconfined condition. Finally, it provides guidance to interpret cell invasion and segregation processes and how these depend on matrix properties.

2.7.2. Dynamic transitions

The dynamics of a cell population has been primarily presented as a function of the motile force, for the sake of simplicity. However, the transitions are primarily controlled by μ/J, reflecting that the balance between cell–cell interactions and cell motile force is what matters. The critical values μ_{c} and μ_{s} at which the qualitative transitions occur depend on other physical and biological parameters involved in this model. For instance, μ_{c} increases with J (figure 2) and decreases with the persistence time τ. As a result, transitions can be triggered by a variation of adhesion, cortical tension or response time as much as by a change in motile force μ.

The concept of dynamical transition, though common in physical systems, has a number of additional implications in a biological context. The results presented here show that minute variations of cellular and environmental parameters can trigger transitions between well-defined phenotypes at the population scale (epithelium/sheet migration/mesenchyme-like, coordinated motion/disordered motion, no/collective/individual invasion). This might explain why such changes in phenotype are often difficult to associate with a proper lineage transition (or a change in gene expression) and how they depend on external parameters.

This behaviour is, in particular, reminiscent of the epithelial–mesenchymal transition (EMT) in living systems, in which cell behaviour changes rapidly from non-migratory to migratory. The causes of such a transition *in vivo* are still highly debated [38,39]. Although a large number of oncogenes are involved, the EMT does not seem to be associated with a proper lineage switch and appears to be very sensitive to environmental conditions. A plausible explanation might be found in the strong nonlinearity of the dynamics observed in this simple model.

2.7.3. Biomolecular signalling

Highly organized behaviours are emerging without the need for specific cues of inter-cellular communications; this raises a number of questions concerning the role of known signalling pathways identified in association with individual or collective cell migration [40]. Cell–cell signalling might be seen either as a complementary (or reinforcing) mechanism, or as a way to compensate for collective effects. While any conclusions at this stage would be speculative, one might already comment on a few well-established facts. Malignant fibroblasts have a reduced contact inhibition of locomotion (CIL) compared with non-malignant fibroblasts [41]. One could question first why normal fibroblasts need CIL, and a possible answer lies in the phenomena of dynamic segregation. As demonstrated by figure 5, unless specific mechanisms are in place, motile fibroblasts would have a spontaneous tendency to stream and segregate rather than disperse in the tissue. CIL might therefore be a necessary behaviour to avoid segregation. This could also explain why changes in CIL can influence the emergence of collective effects in cell populations [4], and, in particular, help tumour cell invasion. By suggesting generic physical mechanisms for collective behaviours, the study shifts the biological questions towards the understanding of how populations of motile cells accurately control their dynamic state in critical parts of development and tissue homeostasis. A number of current signalling mechanisms might have emerged from such evolutionary constraints.

3. MATERIAL AND METHODS

3.1. Numerical model

These simulations are implemented using the CPM [25]. The CPM is a lattice model: the state of the tissue is discrete, represented by an image of the system where the pixel value $\boldsymbol{\sigma}(x, y)$ codes for the identity of the cell covering the location (x, y) in the lattice. Cells can *a priori* adopt any shape on the lattice. The dynamics is introduced by minimizing an energy function E of the state $\boldsymbol{\sigma}(x, y)$ and other physical and biological parameters of the system. Adhesion and cortical tension are accounted for by a single parameter J that provides an energy cost per unit of membrane length (in two-dimensional) between cells. The cell volume is constrained to a reference value v_0, with a compressibility $\boldsymbol{\kappa}^{-1}$. The energy function is minimized using a Monte Carlo process, i.e. by randomly choosing one pixel at a time and testing whether the energy can be lowered by reallocating that pixel to a neighbouring cell. If the energy change ΔE associated with the pixel change is negative, then the move is accepted; if it is positive, then it is accepted with a probability $\exp(-\Delta E/T)$, where T is a parameter accounting for the noise magnitude in the dynamics. Time is expressed in MCS, where 1 MCS corresponds to an average of one iteration per pixel over the whole lattice.

3.2. Motile force

Each cell generates a motile force along its polarization direction $\boldsymbol{n}_i$, with a strength $\boldsymbol{\mu}_i$. These forces are acting between each cell and its substrate (interactions between cells are accounted for by the membrane tension J). To introduce motility in the CPM, the energy function E contains, for each cell i, a time-dependent spatial gradient along $\boldsymbol{n}_i$. These terms essentially act as sources of energy that can drive cell motility. The overall energy function E can be written as

$$E = \underbrace{\Sigma_i \frac{1}{2}\boldsymbol{\kappa}(v_i - v_0)^2}_{\text{volume constraint}} + \underbrace{\Sigma_{k,l} J(1 - \delta_{\sigma(k),\sigma(l)})}_{\text{cell}-\text{cell interactions}} - \underbrace{\Sigma_i \boldsymbol{\mu}_i \boldsymbol{n}_i \cdot \boldsymbol{r}_i}_{\text{cell migration}} \tag{3.1}$$

where sums over i are sums over all cells, and pairs (k,l) represent neighbouring pixels. $\delta_{\sigma(k),\sigma(l)}$ is 1 when the two pixels belong to the same cell, and 0 otherwise. $\boldsymbol{r}_i$ represents the position of the cell's centre of mass.

In a CPM, a constant gradient in the energy function leads to a constant cell velocity, resulting in an effective viscous friction force between the cells and the substrate. The mean cell speed within the epithelium is mostly a linear function of $\boldsymbol{\mu}/J$ for the range of motile forces used here. The origin of the viscous dissipation lies in the Monte Carlo process itself. J controls the amplitude of the membrane fluctuations, which, in turn controls cell diffusion in the absence of a motile force. Migration is induced by a directional bias on membrane fluctuations. When a force is added to the cell, its susceptibility to move is related to its fluctuation dynamics, according to the fluctuation–dissipation theorem, which results in a drag force being inversely proportional to the diffusion coefficient (Stokes–Einstein). In such a Potts model, the dynamics is therefore implicitly overdamped.

3.3. Dynamics of the cell polarity

The direction $\boldsymbol{n}$ of the motile force is determined by a feedback from its earlier displacements (unless specified

otherwise, for instance concerning leader cells). $\boldsymbol{n}$ is oriented along the mean velocity of the cell over its past τ time steps:

$$\boldsymbol{n}_i(t) = \frac{\langle \boldsymbol{v}_i \rangle_{[t-\tau,t]}}{|\langle \boldsymbol{v}_i \rangle_{[t-\tau,t]}|}. \tag{3.2}$$

The parameter τ characterizes the time scale at which cell polarity evolves and integrates changes in the cell's mechanical environment, such as contact with boundaries or with other cells.

3.4. Parameters used

The simulations presented here have been performed using next-nearest neighbour interactions in the energy calculation, a preferred cell area (v_0) of 400 pixels (20×20), an energy fluctuation scale $T = 2.5$, a compressibility $\kappa^{-1} = 0.5$ and a memory time $\tau = 10$ MCS. The results of figure 3 have also been reproduced using next-next-nearest neighbour interactions, using up to 6400 cells. The initial state of the system corresponds to a regular tessellation of the substrate, with each cell starting with a random orientation of its polarization.

3.5. Spatial correlations of the velocity field

The analytical expression of spatial correlation function $g(\delta \boldsymbol{r})$ is

$$g(\delta \boldsymbol{r}) = \frac{\langle \boldsymbol{v}(\boldsymbol{r}) \cdot \boldsymbol{v}(\boldsymbol{r} + \boldsymbol{R}(\boldsymbol{r})\delta \boldsymbol{r}) \rangle_r}{\langle v^2 \rangle_r}, \tag{3.3}$$

where $\boldsymbol{R}(\boldsymbol{r})$ is the rotation matrix turning the x-axis along the direction of $\boldsymbol{v}(\boldsymbol{r})$, so that $\boldsymbol{R}(\boldsymbol{r})\delta \boldsymbol{r}$ is always oriented in the same way with respect to $\boldsymbol{v}(\boldsymbol{r})$, whatever $\boldsymbol{r}$ be, for a given $\delta \boldsymbol{r}$. The rotation therefore ensures that averaging preserves the orientational information, as seen in figure 1*b*; $g(x\boldsymbol{e_x})$ quantifies the correlation along the cell's direction of migration, while $g(y\boldsymbol{e_y})$ characterizes the correlations in the direction transverse to the cell migration.

The λ_c quantifies the width of the domains represented in figure 1*b*. Its value is set to twice the standard deviation of $g(x, y = 0)$:

$$\lambda_c = 2\sqrt{\frac{\int x^2\, g(x,0)\, \mathrm{d}x}{\int g(x,0)\, \mathrm{d}x}}.$$

This work was supported by Engineering and Physical Sciences Research Council (EP/F058586/1). The author thanks R. Adams' group, G. Charras, A. Czirok, G. Gregoire, P. Hersen, B. Ladoux, L. Mahadevan, R. Mayor, E. Sahai and B. Sanson for their valuable comments on this work.

REFERENCES

1 Butler, L. C., Blanchard, G. B., Kabla, A. J., Lawrence, N. J., Welchman, D. P., Mahadevan, L., Adams, R. J. & Sanson, B. 2009 Cell shape changes indicate a role for extrinsic tensile forces in *Drosophila* germ-band extension. *Nat. Cell Biol.* **11**, 859–864. (doi:10.1038/ncb1894)

2 Keller, R., Davidson, L., Edlund, A., Elul, T., Ezin, M., Shook, D. & Skoglund, P. 2000 Mechanisms of convergence and extension by cell intercalation. *Phil. Trans. R. Soc. Lond. B* **355**, 897–922. (doi:10.1098/rstb.2000.0626)

3 Concha, M. L. & Adams, R. J. 1998 Oriented cell divisions and cellular morphogenesis in the zebrafish gastrula and neurula: a time-lapse analysis. *Development* **125**, 983–994.

4 Carmona-Fontaine, C., Matthews, H. K., Kuriyama, S., Moreno, M., Dunn, G. A., Parsons, M., Stern, C. D. & Mayor, R. 2008 Contact inhibition of locomotion *in vivo* controls neural crest directional migration. *Nature* **456**, 957–961. (doi:10.1038/nature07441)

5 Lecaudey, V., Cakan-Akdogan, G., Norton, W. H. & Gilmour, D. 2008 Dynamic Fgf signaling couples morphogenesis and migration in the zebrafish lateral line primordium. *Development* **135**, 2695–705. (doi:10.1242/dev.025981)

6 Friedl, P. & Wolf, K. 2010 Plasticity of cell migration: a multiscale tuning model. *J. Cell Biol.* **188**, 11–19. (doi:10.1083/jcb.200909003)

7 Friedl, P. & Gilmour, D. 2009 Collective cell migration in morphogenesis, regeneration and cancer. *Nat. Rev. Mol. Cell. Biol.* **10**, 445–457. (doi:10.1038/nrm2720)

8 Weijer, C. J. 2009 Collective cell migration in development. *J. Cell Sci.* **122**, 3215–3223. (doi:10.1242/jcs.036517)

9 Deisboeck, T. S. & Couzin, I. D. 2009 Collective behaviour in cancer cell populations. *BioEssays* **31**, 190–197. (doi:10.1002/bies.200800084)

10 Couzin, I. D. & Krause, J. 2003 Self-organization and collective behavior in vertebrates. *Adv. Stud. Behav.* **32**, 1–75. (doi:10.1016/S0065-3454(03)01001-5)

11 Zhang, H. P., Beer, A., Florin, E. L. & Swinney, H. L. 2010 Collective motion and density fluctuations in bacterial colonies. *Proc. Natl Acad. Sci. USA* **107**, 13 626–13 630. (doi:10.1073/pnas.1001651107)

12 Schaller, V., Weber, C., Semmrich, C., Frey, E. & Bausch, A. 2010 Polar patterns of driven filaments. *Nature* **467**, 73–77. (doi:10.1038/nature09312)

13 Vicsek, T., Czirok, A., Ben-Jacob, E., Cohen, I. & Shochet, O. 1995 Novel type of phase transition in a system of self-driven particles. *Phys. Rev. Lett.* **75**, 1226–1229. (doi:10.1103/PhysRevLett.75.1226)

14 Grégoire, G. & Chaté, H. 2004 Onset of collective and cohesive motion. *Phys. Rev. Lett.* **92**, 025702. (doi:10.1103/PhysRevLett.92.025702)

15 Szabo, B., Szöllösi, G. J., Gönci, B., Jurányi, Zs., Selmeczi, D. & Vicsek, T. 2006 Phase transition in the collective migration of tissue cells: experiments and model. *Phys. Rev. E* **74**, 061908. (doi:10.1103/PhysRevE.74.061908)

16 Szabo, A., Ünnep, R., Méhes, E., Twal, W. O., Argraves, W. S., Cao, Y. & Czirók, A. 2010 Collective cell motion in endothelial monolayers. *Phys. Biol.* **7**, 046007. (doi:10.1088/1478-3975/7/4/046007)

17 Belmonte, J. M., Thomas, G. L., Brunnet, L. G., de Almeida, R. M. C. & Chaté, H. 2008 Self-propelled particle model for cell-sorting phenomena. *Phys. Rev. Lett.* **100**, 248702. (doi:10.1103/PhysRevLett.100.248702)

18 Haga, H., Irahara, C., Kobayashi, R., Nakagaki, T. & Kawabata, K. 2005 Collective movement of epithelial cells on a collagen gel substrate. *Biophys. J.* **88**, 2250–2256. (doi:10.1529/biophysj.104.047654)

19 Poujade, M., Grasland-Mongrain, E., Hertzog, A., Jouanneau, J., Chavrier, P., Ladoux, B., Buguin, A. & Silberzan, P. 2007 Collective migration of an epithelial monolayer in response to a model wound. *Proc. Natl Acad. Sci. USA* **104**, 15 988–15 993. (doi:10.1073/pnas.0705062104)

20 Vitorino, P. & Meyer, T. 2008 Modular control of endothelial sheet migration. *Genes Dev.* **22**, 3268–3281. (doi:10.1101/gad.1725808)

21 Angelini, T. E., Hannezo, E., Trepat, X., Fredberg, J. J. & Weitz, D. A. 2010 Cell migration driven by cooperative substrate deformation patterns. *Phys. Rev. Lett.* **104**, 168104. (doi:10.1103/PhysRevLett.104.168104)

22 Angelini, T. E., Hannezob, E., Trepatc, X., Marquezd, M., Fredberge, J. J. & Weitzf, D. A. 2011 Glass-like dynamics of collective cell migration. *Proc. Natl Acad. Sci. USA* **108**, 4714–4719. (doi:10.1073/pnas.1010059108)

23 Tambe, D. T. *et al.* 2011 Collective cell guidance by cooperative intercellular forces. *Nat. Mat.* **10**, 469–475. (doi:10.1038/nmat3025)

24 Krieg, M., Arboleda-Estudillo, Y., Puech, P.-H., Käfer, J., Graner, F., Müller, D. J. & Heisenberg, C.-P. 2008 Tensile forces govern germ-layer organization in zebrafish. *Nat. Cell Biol.* **10**, 429–436. (doi:10.1038/ncb1705)

25 Graner, F. & Glazier, J. A. 1992 Simulation of biological cell sorting using a two-dimensional extended Potts model. *Phys. Rev. Lett.* **69**, 2013–2016. (doi:10.1103/PhysRevLett.69.2013)

26 McCann, C. P., Kriebel, P. W., Parent, C. A. & Losert, W. 2010 Cell speed, persistence and information transmission during signal relay and collective migration. *J. Cell Sci.* **123**, 1724–1731. (doi:10.1242/jcs.060137)

27 Van Haastert, P. J. M. 2010 Chemotaxis: insights from the extending pseudopod. *J. Cell Sci.* **123**, 3031–3037. (doi:10.1242/jcs.071118)

28 Vedula, S. R. K. *et al.* In press. Emerging modes of collective cell migration induced by geometrical constraints. *Proc. Natl Acad. Sci. USA*. (doi:10.1073/pnas.1119313109)

29 Gaggioli, C., Hooper, S., Hidalgo-Carcedo, C., Grosse, R., Marshall, J. F., Harrington, K. & Sahai, E. 2007 Fibroblast-led collective invasion of carcinoma cells with differing roles for RhoGTPases in leading and following cells. *Nat. Cell Biol.* **9**, 1392–1400. (doi:10.1038/ncb1658)

30 Petitjean, L., Reffay, M., Grasland-Mongrain, E., Poujade, M., Ladoux, B., Buguin, A. & Silberzan, P. 2011 Velocity fields in a collectively migrating epithelium. *Biophys. J.* **98**, 1790–1800. (doi:10.1016/j.bpj.2010.01.030)

31 Reffay, M., Petitjean, L., Coscoy, S., Grasland-Mongrain, E., Amblard, F., Buguin, A. & Silberzan, P. 2011 Orientation and polarity in collectively migrating cell structures: statics and dynamics. *Biophys. J.* **100**, 2566–2575. (doi:10.1016/j.bpj.2011.04.047)

32 Ouaknin, G. Y. & Bar-Yoseph, P. Z. 2009 Stochastic collective movement of cells and fingering morphology: no maverick cells. *Biophys. J.* **97**, 1811–1821. (doi:10.1016/j.bpj.2009.05.064)

33 Mark, S., Shlomovitz, R., Gov, N. S., Poujade, M., Grasland-Mongrain, E. & Silberzan, P. 2010 Physical model of the dynamic instability in an expanding cell culture. *Biophys. J.* **98**, 361–370. (doi:10.1016/j.bpj.2009.10.022)

34 Lee, P. & Wolgemuth, C. W. 2011 Crawling cells can close wounds without purse strings or signaling. *PLoS Comput. Biol.* **7**, pe1002007.

35 Couzin, I. D., Krause, J., Franks, N. R. & Levin, S. A. 2005 Effective leadership and decision-making in animal groups on the move. *Nature* **433**, 513–518. (doi:10.1038/nature03236)

36 Trepat, X., Wasserman, M. R., Angelini, T. E., Millet, E., Weitz, D. A., Butler, J. P. & Fredberg, J. J. 2009 Physical forces during collective cell migration. *Nat. Phys.* **5**, 426–430. (doi:10.1038/nphys1269)

37 Mehes, E., Mones, E., Nemeth, V. & Vicsek, T. 2012 Collective motion of cells mediates segregation and pattern formation in co-cultures. *PLoS ONE* **7**, pe31711. (doi:10.1371/journal.pone.0031711)

38 Tarin, D. 2005 The fallacy of epithelial mesenchymal transition in neoplasia. *Cancer Res.* **65**, 5996. (doi:10.1158/0008-5472.CAN-05-0699)

39 Thiery, J. P. & Sleeman, J. P. 2006 Complex networks orchestrate epithelial–mesenchymal transitions. *Nature* **7**, 131–142. (doi:10.1038/nrm1835)

40 Affolter, M. & Weijer, C. J. 2005 Signaling to cytoskeletal dynamics during chemotaxis. *Dev. Cell* **9**, 19–34. (doi:10.1016/j.devcel.2005.06.003)

41 Abercrombie, M. 1979 Contact inhibition and malignancy. *Nature* **281**, 259–62. (doi:10.1038/281259a0)